Articles

Preparation, Spectroscopic Characterization, and Frontier MO Study of the Heteronuclear Luminescent [Pt₂Au₂(dmb)₂(PPh₃)₄](PF₆)₂ Cluster (dmb = 1,8-Diisocyano-*p*-menthane). A Cluster with a Formal Au⁰−Au⁰ Bond Encapsulated inside a "Pt₂(dmb)₂²⁺ " Fragment

Tianle Zhang, Marc Drouin, and Pierre D. Harvey*

Département de chimie, Université de Sherbrooke, Sherbrooke, Québec, Canada J1K 2R1

Received October 6, 1998

The title compound is prepared from the direct reaction of $Pt_2(dba)_3$ (dba = dibenzylideneacetone) and [Au-$(PPh_3)_2](PF_6)$ in the presence of 1,8-diisocyano-*p*-methane (dmb), with $Pt_2(dmb)_2Cl_2$, $[Pt_4(dmb)_4(PPh_3)_2](PF_6)_2$, and $(PPh_3)AuCl$ being formed as parallel products. X-ray crystallography reveals the presence of a quasi-linear $PPh_3Au-AuPPh_3$ fragment encapsulated inside a "$Pt_2(dmb)_2^{2+}$" ring which is axially coordinated with two PPh_3 ligands. The d(AuAu) is 2.5977(6) Å and is indicative of a strong Au−Au single bond. The IR ν(CN) data reveal that the Pt oxidation state is I, which places the Au oxidation state at 0. The PtAu distances are 2.8422(5) and 2.8082(5) Å. The Raman-active $\nu(Au_2)$, ν(PtAu) ($b_{2g} + a_g$), ν(PtP), ν(AuP), and ν(PtC) are found at 121.2, ∼100, 85.5, 162.1, 183.1, and 457.2, and 440.9 cm⁻¹, respectively. The PtAu (0.67 mdyn Å⁻¹) and Au_2 (1.21 mdyn Å⁻¹) force constants (F) confirm the presence of medium PtAu and strong Au_2 bonding interactions. The absorption spectra are characterized by strong bands at λ_{max} (ϵ, M⁻¹ cm⁻¹) at 316 (32 300), 366 (37 800), and 418 nm (21 500) and lower intensity features at 516 (2860) and 655 nm (834). The cluster is luminescent at low temperatures (solid and frozen glasses), and in the solid state at room temperature, and exhibits an emission band at ∼875 nm, and an emission lifetime, τ_e, of 4.4 ± 0.4 ns (solvent = butyronitrile, T = 77 K).

Introduction

Heteronuclear Pt−Au clusters have been the topic of increasing interest over the past 10 years or so.[1] These clusters exhibit very rich chemistry and a very wide variety of structures and polynuclearity, where both the Pt−Au bonding and related reactivity are at the center of attention. Some time ago Mingos et al. reported the preparation and X-ray structure of an unusual heteronuclear [Au₂Pt₂(PPh₃)₄(CN-xylyl)₄](PF₆)₂ cluster (Chart 1), where the structure is defined as a flattened butterfly with the gold atoms occupying the edge-sharing bond.[2] This structure was unusual because the Pt−Au distances were separated into two groups, short ones (2.718(2) and 2.712(2) Å) and long ones (2.922(2) and 3.028(2) Å).[2] The authors tentatively explained this structure by claiming the presence of a mixed-valence Auᴵ−

Chart 1

R = xylyl
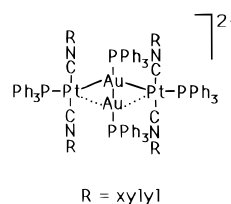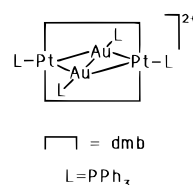
Chart 2

▢ = dmb

L = PPh₃

Auᴵᴵᴵ bond, somewhat supported from EHMO calculations.[3] If such a limiting case were true, then the remaining Pt metals would carry a −1 charge, which is an unusual oxidation state for Pt, and more unlikely, if the surrounding ligands are poorer π-acceptors such as isocyanides and phosphines. We now report a new example of such a cluster, [Pt₂Au₂(dmb)₂(PPh₃)₄](PF₆)₂ (dmb = 1,8-diisocyano-*p*-methane) (Chart 2), except that evidence for a Au(0)−Au(0) single bond will be provided, leaving the residual positive charge on the Pt (i.e., Pt(I)). Although the most common oxidation states for Au are +1 and

(1) See, for examples: (a) Krogstad, D. A.; Konze, W. V.; Pignolet, L. H. *Inorg. Chem.* **1996**, *35*, 6763. (b) Rubinstein, L. I.; Pignolet, L. H. *Inorg. Chem.* **1996**, *35*, 6755. (c) Pignolet, L. H.; Aubart, M. A.; Craighead, K. L.; Gould, R. A. T.; Korgstad, D. A.; Wiley: J. S. *Coord. Chem. Rev.* **1995**, *143*, 219. (d) Kappen, G.; Smits, J. M. M.; Beurskens, P. T.; Steggerda, J. J. *Inorg. Chem.* **1995**, *34*, 2121. (e) Kappen, T. G. M. M.; Schlebos, P. P. J.; Bour, J. J.; Bosman, W. P.; Smits, J. M. M.; Beurskens, P. T.; Steggerda, J. J. *Inorg. Chem.* **1995**, *34*, 2133. (f) Gould, R. A. T.; Craighead, K. L.; Wiley, J. S.; Pignolet, L. H. *Inorg. Chem.* **1995**, *34*, 2902. (g) Laupp, M.; Strähle, J. *Angew. Chem., Int. Ed. Engl.* **1994**, *33*, 207. (h) Teo, B. K.; Zhang, H. *Coord. Chem. Rev.* **1995**, *143*, 611.

(2) (a) Briant, C. E.; Gilmour, D. I.; Mingos, D. M. P. *J. Organomet. Chem.* **1984**, *267*, C52. (b) Briant, C. E.; Mingos, D. M. P. *J. Chem. Soc., Dalton Trans.* **1986**, 835.

(3) Gilmour, D. I.; Mingos, D. M. P. *J. Organomet. Chem.* **1986**, *302*, 127.

+3, several examples of clusters exhibiting an average formal oxidation state <+1 exist.[4] Common examples for such clusters include core fragments of the type Au_4^{2+}, Au_8^{2+}, Au_{11}^{3+}, etc. These species exhibit a large range of Au−Au bond lengths, some of which can be as low as 2.600−2.625 Å, clearly indicating strong bonding. The title compound is interesting for three reasons. First, to our knowledge, this cluster exhibits one of the shortest Au−Au single bonds ever reported. Second, this is the first example of a M−M bond that is encapsulated/encircled inside an organometallic fragment (i.e., "Pt₂(dmb)₂²⁺"). Third, this cluster is luminescent, and its emission band is the lowest energy band (λ_{max} ∼875 nm at 12 K) ever reported for a M₄ compound.

Experimental Section

Materials. Pt₂(dba)₃·CHCl₃,[5] dmb,[6] and [Au(PPh₃)₂](PF₆)[7] were prepared according to standard procedures. All reagents (PPh₃, K₂PtCl₄, HAuCl₄, SEt₂, AgNO₃, NH₄PF₆, NaO₂CCH₃) were from Aldrich and were used without purification. All experiments were carried out under a N₂ atmosphere. Solvents for spectroscopic measurements were purified according to procedures outlined in ref 8.

[Pt₂Au₂(dmb)₂(PPh₃)₄](PF₆)₂. To a suspension of Pt₂(dba)₃·CHCl₃ (0.0545 g, 0.0045 mmol) in 6 mL of acetone was added 0.0740 g (0.039 mmol) of dmb, and the mixture was stirred under a nitrogen atmosphere for 3 h. The black solid was slowly dissolved to give a yellow-orange solution. The solution was filtered, and then diethyl ether was added to precipitate the reactive intermediate material (0.0366 g, 0.020 mmol), {[Pt₄(dmb)₅]Cl₂}ₙ, which was collected by filtration and washed with diethyl ether. This red-orange solid was inserted immediately into a 50 mL flask, which was purged with nitrogen for 30 min. A mixture of methanol (1 mL) and acetone (3 mL) was then added by a syringe to dissolve the solid to give a yellow-orange solution, to which 1 mL of an acetone solution of [Au(PPh₃)₂](PF₆) (0.0183 g, 0.021 mmol) was added. The solution turned brown in a few minutes and subsequently turned yellow-brown in 2 h. The solution was filtered and evaporated to about 2 mL. The yellow-green crude product was collected by precipitation with diethyl ether and filtration (0.0420 g). This crude product was then dissolved in dichloromethane to give a deep green solution and a solid material, Pt₂(dmb)₂Cl₂, which was identified by spectroscopic comparison with an authentic sample (∼0.0250 g). The crystallization of the deeply colored solution provided orange crystals ([Pt₄(dmb)₄(PPh₃)₂](PF₆)₂) and dark green crystals ([Pt₂Au₂(dmb)₂(PPh₃)₄](PF₆)₂). The identification of the green product ([Pt₂Au₂(dmb)₂(PPh₃)₄](PF₆)₂) was made from crystallography. The identification of the other products was made from spectroscopic comparison of an authentic sample for Pt₂(dmb)₂Cl₂, and from the comparison of a very closely related salt for [Pt₄(dmb)₄(PPh₃)₂](PF₆)₂ ([Pt₄(dmb)₄(PPh₃)₂]Cl₂).

The characterization details of the products and authentic samples are presented below.

[Pt₂Au₂(dmb)₂(PPh₃)₄](PF₆)₂. FAB mass: calcd for [Pt₂Au₂(dmb)₂(PPh₃)₄]PF₆ 2358.9, obsd ∼2360 m/e (rel int ∼3%); calcd for [Pt₂Au₂(dmb)₂(PPh₃)₄] 2213.9, obsd 2214.9 m/e (rel int 8%); calcd for [Pt₂Au₂(dmb)₂(PPh₃)₃] 1951.5, obsd 1951.6 m/e (rel int 46%); calcd for [Pt₂Au(dmb)₂(PPh₃)] 1230.0, obsd 1230.4 (rel int 100%). IR (solid): 2164 cm⁻¹ (ν(C≡N)). ¹H NMR (CD₂Cl₂): δ 0.6−1.6 ppm (complex, 36H, dmb), 7.1−7.6 ppm (complex, 60H, PPh₃). ³¹P NMR (CD₂Cl₂): δ 44.80 ppm [Au−P] (¹J(Pt−P) = 2253 Hz, ³J(Pt−P) =

395 Hz), 59.0 ppm [Pt−P] (²J(Pt−P) = 147 Hz, ³J(PP) = 17 Hz). UV−vis (CH₂Cl₂): λ_{max} 316, 366, 420, 518, 654 nm. The dark-green crystals suitable for crystallography were grown from a solution in a mixture of CH₂Cl₂ and cyclohexane.

[Pt₄(dmb)₄(PPh₃)₂](PF₆)₂. Mass FAB: calcd for [Pt₄(dmb)₄(PPh₃)₂]-(PF₆)₂ 2356.1, obsd 2358 m/e (rel int 5%); calcd for [Pt₄(dmb)₄(PPh₃)₂]-(PF₆) 2210, obsd 2211.1 (rel int 75%). IR (solid): 2146 cm⁻¹ (ν(C≡N)), 841 cm⁻¹ (ν(PF₆⁻)). ¹H NMR (acetone-d₆): δ 1.0−2.1 ppm (complex, dmb), 7.2−7.6 ppm (complex, PPh₃). UV−vis (CH₃CN): λ_{max} 298, 358, 406, 518 nm.

Pt₂(dmb)₂Cl₂. Anal. (Calcd for C₂₄H₃₆N₄Cl₂Pt₂·(C₂H₅)₂O: C, 36.72; H, 4.31; N, 6.12. Found: C, 36.60; H, 4.78; N, 6.58. Mass FAB: calcd for Pt₂(dmb)₂ 770.8, obsd 770 (rel int ∼3%); calcd for Pt₂(dmb)Cl 615.9, obsd 615 (rel int ∼5%). IR (solid): 2180, 2160 cm⁻¹ (ν(C≡N). UV−vis (CH₃CN): λ_{max} 300 (s), 314 (shoulder), 404 (w) nm. ¹H NMR (CD₃CN): δ 1.0−2.1 (complex, dmb).

Pt₂(dmb)₂Cl₄. This compound was prepared according to a literature procedure for Pd₂(dmb)₂Cl₄ adapted for Pt.[9] Solid K₂PtCl₄ (0.50 g, (1.205 mmol) was dissolved in 10 mL of distilled water. To this solution was added 0.33 g (1.740 mmol) of solid dmb. This mixture was stirred for 5 h. Then a yellow product was collected by filtration and washed with distilled water and diethyl ether. The crude solid was slowly recrystallized from acetonitrile/diethyl ether solution. Yield: 0.18 g, 33%. Anal. (Calcd for C₂₄H₃₆N₄Cl₄Pd₂·2CH₃CN: C, 33.81; H, 4.26; N, 8.44. Found: C, 33.94; H, 4.52; N, 8.77. IR (solid): 2221 cm⁻¹ (ν(C≡N). UV−vis (CH₃CN): λ_{max} 196 (s), 258 (m), 352 (w), 464 nm (m). The presence of crystallization molecules was confirmed by ¹H NMR. ¹H NMR (CD₃CN): δ 1.2−1.8 (complex, dmb). FAB mass: calcd for Pt₂(dmb)(dmb-CN)Cl₃ 851.1, obsd 849.2 (rel int <1%); calcd for Pt₂(dmb-CN)Cl₃ 825.1, obsd 824.0 (rel int <1%); calcd for Pt₂(dmb)₂Cl 806.2, obsd 805.0 m/e (rel int <1%). dmb-CN is dmb that has lost a CN group.

Pt₂(dmb)₂Cl₂. This compound was prepared according to a literature procedure for Pd₂(dmb)₂Cl₂ adapted for Pt.[9] Solid Pt₂(dba)₃·CHCl₃ (0.0301 g, 0.025 mmol) was dissolved in 10 mL of benzene, to which was added 0.0260 g (0.028 mmol) of Pt₂(dmb)₂Cl₄ dissolved in 10 mL of acetonitrile in the presence of an excess of dmb (0.031 g, 0.163 mmol). The color of the solution changed from purple to brown. Then the solution was evaporated to dryness and washed with diethyl ether. This solid was redissolved in 5 mL of acetonitrile and then filtered to remove the insoluble species. The product was precipitated with diethyl ether, collected by filtration, and washed with diethyl ether. Yield: 0.0299 g, 64.6%. Anal. (Calcd for C₂₄H₃₆N₄Cl₂Pt₂·2CH₃CN·((C₂H₅)₂O): C, 38.51; H, 5.25; N, 8.42. Found: C, 38.37; H, 5.15; N, 8.11. The presence of crystallization molecules was confirmed by ¹H NMR. IR (solid): 2182, 2155 cm⁻¹ (ν(C≡N)). UV−vis (CH₃CN): λ_{max} 300 (s), 316 (s, shoulder), 406 (w) nm. ¹H NMR (CD₃CN): δ 1.0−1.8 (complex, dmb). Mass FAB: calcd for Pt₂(dmb)₂Cl₂ 841.7, obsd 841 (very weak); calcd for Pt₂(dmb)₂ 770.8, obsd 771 m/e (rel int <1%).

X-ray Crystallography. Intensity data were collected at 293 K on an Enraf-Nonius CAD-4 automatic diffractometer using graphite-monochromated Cu Kα radiation. The DIFFRAC program was used for centering, indexing, and data collection. The unit cell dimensions were obtained by least-squares fitting of 10 centered reflections in the range 20° ≤ 2θ ≤ 30°. During data collection, the intensities of two standard reflections were monitored every 60 min. No significant decay was observed. An absorption correction was applied on the data based on ψ-scan measurements on 9 azimuthal reflections. The minimum and maximum transmission factors were 0.0118 and 0.1129. The structure was solved by the application of direct methods using the SOLVER program from NRCVAX[10] and refined by least-squares using the SHELXL-97[11] program. At convergence the final discrepancy indices were R1 = 0.0447, wR2 = 0.1305, S = 1.093. The residual

(4) (a) Copley, R. C. B.; Mingos, D. M. P. *J. Chem. Soc., Dalton Trans.* **1996**, 479. (b) Crespo, O.; Gimeno, M. C.; Jones, P. G.; Laguna, A.; Villacampa, M. D. *Angew. Chem., Int. Ed. Engl.* **1997**, *36*, 993.

(5) Maitlis, P. M.; Moseley, K. *J. Chem. Soc., Chem. Commun.* **1971**, 982.

(6) Weber, W. P.; Gokel, G. W.; Ugi, I. K. *Angew. Chem., Int. Ed. Engl.* **1972**, *11*, 530.

(7) Sykes, A. G.; Mann, K. R. *J. Am. Chem. Soc.* **1990**, *112*, 7247.

(8) (a) Perrin, D. D.; Armarego, W. L. F.; Perrin, D. R. *Purification of Laboratory Chemicals*; Pergamon: Oxford, U.K., 1966. (b) Gordon, A. J.; Ford, R. A. *The Chemist's Companion, A Handbook of Practical Data, Techniques, and References*; Wiley: New York, 1972; p 436.

(9) Perreault, D.; Drouin, M.; Michel, A.; Harvey, P. D. *Inorg. Chem.* **1992**, *31*, 2740.

(10) (a) Le Page, Y.; White, P. S.; Gabe, E. J. *NRCCAD, An enhanced CAD-4 Control Program, Proc. Am. Crystallogr.*, Hamilton Meeting, 1986; Abstract PA23. (b) Gabe, E. J.; Le Page, Y.; Charland, J.-P.; Lee, F. L.; White, P. S. *J. Appl. Crystallogr.* **1989**, *22*, 384.

(11) Sheldrick, G. *SHELX-97*; Institut Anorg. Chemie: Tammannstr. 4, D37077, Göttingen, Germany, 1997.

Chart 3
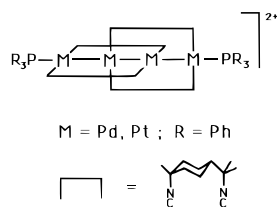
positive and negative electron densities in the final maps were located in the vicinity of the Pt and Au atoms. All non-H atoms were refined anisotropically. The H atoms were geometrically placed. The dmb ligands are disordered. The occupancy refinement converged to 0.459-(8)/0.541(8). There are two phenyl rings which show disorder. The respective occupancies for C32−C36 and C37−C42 are 0.311(11)/0.689(11) and 0.699(9)/0.301(9).

Instruments. The UV−vis spectra were recorded on a Hewlett-Packard 8452A diode array spectrometer. The chemical analysis measurements were performed at the Université de Montréal for C, H, N. The mass spectra were acquired using a Kratos MS50 TCTA spectrometer using an Iontech saddle field source model FAB 11NF operating at 70 kV with 2 mA current. The samples were in thiolglycerol or NBA matrixes. The FT-IR (4000−600 cm^{-1}) spectra were obtained on a Bomem (MB-102) spectrometer. The Raman spectra at 298 K in the solid state were acquired using a Nd:YAG laser (1064 nm excitation) and a notch filter (cutoff ∼50 cm^{-1}). The luminescence spectra were obtained on a steady-state LS-100 spectrofluorometer from Photo Technology Inc. or on a Fluorolog II instrument. The detector was a Hamamatsu R508 PMT, for both instruments. The emission lifetimes were measured on the PTI LS100 instrument using a nanosecond photo counting system.

Calculation Details. All of the MO calculations were of the extended Hückel type (EHMO)[12,13] using a modified version of the Wolfsberg−Helmholz formula.[14] The atomic parameters used for C,[13] N,[13] H,[13] P,[15] Pt,[16] and Au[17] were from the literature. Because of limitations in the size of molecules handled by the program, dmb was replaced by two CH$_3$NC, and PPh$_3$ by PH$_3$. Hence the computed molecule is Pt$_2$Au$_2$(CNCH$_3$)$_4$(PH$_3$)$_4$$^{2+}$. This methodology is a standard one.[18] The bond distances and angles are those reported in the X-ray structure (average values). A detailed description of the graphic programs used in this work can be found in ref 19.
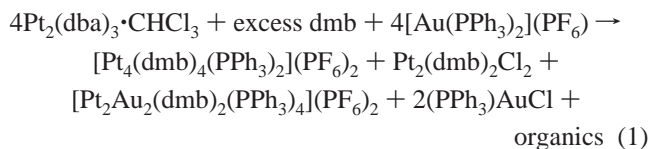
Results and Discussion

1. Preparation and X-ray Structure. Previous works[20] indicated that the M$_2$(dba)$_3$·CHCl$_3$ dimers (M = Pd^0, Pt^0) react with dmb and PPh$_3$ to form the tetranuclear clusters [M$_4$(dmb)$_4$-(PPh$_3$)$_2$]Cl$_2$ (Chart 3, M = Pd, Pt). These M−M bonded clusters exhibit a quasi-linear M$_4$P$_2$ geometry, where a catenate structure is formed using the dmb bridging ligands. Indeed, the dmb ligands bridge two M atoms each to form two interlocking "M$_2$-(dmb)$_2$" rings. These new compounds are formally 58-electron clusters. One of the intermediate reagents in these reactions is the "[Pd$_4$(dmb)$_4$(dmb)]Cl$_2$" polymer, which in one case, the relatively stable polymer {[Pd$_4$(dmb)$_4$(dmb)](CH$_3$CO$_2$)$_2$}$_n$, was formally characterized from X-ray crystallography.[20] By replac-
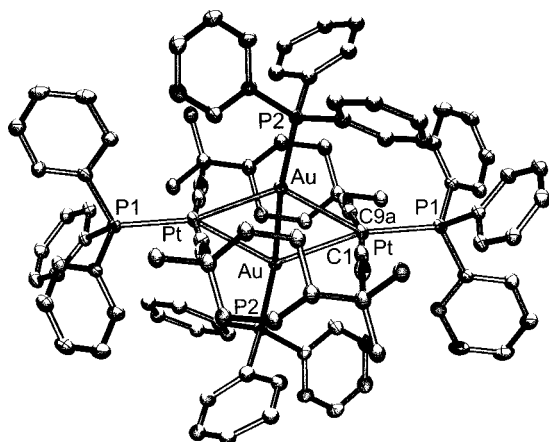
(12) Hoffmann, R.; Lipscomb, W. N. *J. Chem. Phys.* **1962**, *36*, 2179.
(13) (a) Hoffmann, R.; Lipscomb, W. N. *J. Chem. Phys.* **1962**, *36*, 2872. (b) Hoffmann, R. *J. Chem. Phys.* **1963**, *39*, 1397.
(14) Ammeter, J. H.; Burgi, H. B.; Thibeault, J. C.; Hoffmann, R. *J. Am. Chem. Soc.* **1978**, *100*, 3686.
(15) Summerville, R. H.; Hoffmann, R. *J. Am. Chem. Soc.* **1976**, *98*, 7240.
(16) Macchi, P.; Proserpio, D. M.; Sironi, A. *Organometallics* **1997**, *16*, 2101.
(17) Komiya, S.; Albright, T. A.; Hoffmann, R.; Kochi, J. K. *J. Am. Chem. Soc.* **1977**, *99*, 8440.
(18) Mealli, C. *J. Am. Chem. Soc.* **1985**, *107*, 2245.
(19) Mealli, C.; Proserpio, D. M. *J. Chem. Educ.* **1990**, *67*, 399.
(20) (a) Zhang, T.; Drouin, M.; Harvey, P. D. *Inorg. Chem.* **1999**, *38*, 1305. (b) Zhang, T.; Drouin, M.; Harvey, P. D. *Inorg. Chem.* **1999**, *38*, 957.

Table 1. Crystal Data for [Pt$_2$Au$_2$(dmb)$_2$(PPh$_3$)$_4$](PF$_6$)$_2$

empirical formula	C$_{96}$H$_{96}$N$_4$F$_{12}$P$_6$Pt$_2$Au$_2$
fw	2503.98
wavelength, Å	1.54060
cryst syst, space group	triclinic, $P\bar{1}$
unit cell dimens	
a, Å	12.0371(19)
b, Å	14.0188(9)
c, Å	15.3362(11)
α, deg	63.709(5)
β, deg	80.348(7)
γ, deg	86.711(7)
vol, Å^3	2288.6(3)
Z	1
calcd density, Mg/m^3	2.376
θ range, deg	3.25−69.86
reflns collected/unique [R(int) = 0.0000]	8634/8634
data/restraints/params	8634/147/499
final R indices [$I > 2\sigma(I)$]^a	R1 = 0.0447, wR2 = 0.1305
R indices (all data)^a	R1 = 0.0618, wR2 = 0.1418

^{a} R1 = $\sum(||F_o| - |F_c||)/\sum|F_o|$, wR2 = $\{\sum[w(F_o^2 - F_c^2)^2]/\sum w(F_o^2)^2\}^{1/2}$ [$w = 1/(\sigma^2(F_o^2) + 0.1P)^2$ where $P = (F_o^2 + F_c^2)/3$].

ing PPh$_3$ by the bidentate Ph$_2$P(CH$_2$)$_m$PPh$_2$ ligands (m = 4, 5, 6; L−L), a new family of block copolymers ({[Pt$_4$(dmb)$_4$(L-L)]Cl$_2$}$_n$), were also prepared and characterized.[20] In this work, an attempt to make an extended chain of the type Pt$_4$Au$_2$ is made, by replacing the PPh$_3$ reagent with a gold(I) species, notably (PPh$_3$)Au$^+$. Instead the reaction proceeds this way (eq 1):

$$4Pt_2(dba)_3\cdot CHCl_3 + \text{excess dmb} + 4[Au(PPh_3)_2](PF_6) \rightarrow$$
$$[Pt_4(dmb)_4(PPh_3)_2](PF_6)_2 + Pt_2(dmb)_2Cl_2 +$$
$$[Pt_2Au_2(dmb)_2(PPh_3)_4](PF_6)_2 + 2(PPh_3)AuCl +$$
$$\text{organics} \quad (1)$$

All complexes have been formally identified from spectroscopic comparison with authentic or related samples (see Experimental Section), except for the mixed-metal cluster, which was analyzed from X-ray crystallography.

The electrophilic Au(PPh$_3$)$^+$ species are known to react with zerovalent Pt clusters to form mixed-metal compounds.[21,22] The reaction is believed to proceed via an insertion of the d^{10} Au-(PPh$_3$)$^+$ fragment into the M−M bonds. For example, insertion of AuCl and Au(PPh$_3$)$^+$ into the electron-rich M$_2$-bonded Pt$_2$-(dppm)$_2$X$_2$ species (X = Cl, CN) were recently reported.[23,24] According to the [Pt$_4$(dmb)$_4$(PPh$_3$)$_2$]$^{2+}$ X-ray structure,[20] a direct attack of the Au(PPh$_3$)$^+$ fragment onto one of the Pt−Pt bonds is strongly sterically hindered. Instead, a dissociation reaction must occur to generate the isolated and characterized Pt$_2$(dmb)$_2$-Cl$_2$ product and an uncharacterized highly reactive zerovalent Pt intermediate. Dismutation reactions are also not uncommon in low-valent tetranuclear compounds.[25] Similarly the closely related [Pt$_2$Au$_2$(PPh$_3$)$_4$(CNC$_6$H$_3$Me$_2$-2,6)](PF$_6$)$_2$ compound is prepared from the interaction between Au(PPh$_3$)$^+$ and the zerovalent [Pt(PPh$_3$)$_2$(C$_2$H$_4$)] complex.

The X-ray structure of the tetranuclear [Pt$_2$Au$_2$(dmb)$_2$(PPh$_3$)$_4$]-(PF$_6$)$_2$ cluster (Tables 1 and 2) reveals the commonly encoun-

(21) Briant, C. E.; Wardle, R. W. M.; Mingos, D. M. P. *J. Organomet. Chem.* **1984**, *267*, C49.
(22) Mingos, D. M. P.; Wardle, R. W. M. *J. Chem. Soc., Dalton Trans.* **1986**, 73.
(23) Puddephatt, R. J.; Arsenault, G. J. *Can. J. Chem.* **1989**, *67*, 1800.
(24) Toronto, D. V.; Balch, A. L. *Inorg. Chem.* **1994**, *33*, 6132.
(25) Tejel, C.; Ciriano, M. A.; Lopez, J. A.; Lahoz, F. J.; Oro, L. A. *Angew. Chem., Int. Ed.* **1998**, *37*, 1542.

Table 2. Selected Bond Lengths (Å) and Angles (deg) for [Pt$_2$Au$_2$(dmb)$_2$(PPh$_3$)$_4$](PF$_6$)$_2$[a]

Pt−C(1)	1.918(8)	Pt−Aua	2.8422(5)
Pt−C(9a)	1.928(9)	Au−Aua	2.5997(6)
Pt−P(1)	2.3612(19)	Aua−Pta	2.8082(5)
Pt−Au	2.8082(5)	Au−Pta	2.8423(5)
Au−P	2.317(2)		
C(1)−Pt−C(9a)	168.4(4)	P(1)−Pt−Aua	146.16(5)
C(1)−Pt−P(1)	98.6(3)	Au−Pt−Aua	54.738(13)
C(9a)−Pt−P(1)	92.9(3)	P(2)−Au−Aua	172.67(6)
C(1)−Pt−Au	91.2(3)	P(2)−Au−Pt	123.81(5)
C(9a)−Pt−Au	77.7(3)	Aua−Au−Pt	63.297(15)
P(1)−Pt−Au	157.66(5)	P(2)−Au−Pta	110.90(5)
C(1)−Pt−Aua	83.1(3)	Aua−Au−Pta	61.964.(15)
C(9a)−Pt−Aua	87.8(3)	Pt−Au−Pta	125.261(14)

[a] The atom numbering refers to Figure 1. The Au and Aua (and so on) are related by symmetry.

Figure 1. ORTEP drawing of the Pt$_2$Au$_2$(dmb)$_2$(PPh$_3$)$_4{}^{2+}$ cluster. The ellipsoids are shown at 10% probability, and the H atoms are not shown for clarity.

tered 20-membered "Pt$_2$(dmb)$_2$" ring,[26] axially Pt-bonded to two PPh$_3$ ligands, and encapsulating a M$_2$-bonded Ph$_3$PAu−AuPPh$_3$ fragment (Figure 1). The Pt$_2$Au$_2$ frame exhibits a flattened butterfly structure (approximated local symmetry = D_{2h}) where the Au−Au bond is located on the edge-sharing side of this geometry. The d(AuAu) and d(PtAu) data are 2.5977(6) Å, and 2.8082(5) and 2.8423(5) Å, respectively, and indicate a strong Au−Au bonding, and medium Pt−Au interactions. The d(PtC) data are normal (Table 2). In addition, the dmb bite distance is 5.02 Å, a distance that compares favorably to that found in polymers of the type {[Ag(dmb)$_2$]Y}$_n$ (bite distance ∼5 Å; Y = PF$_6{}^-$, BF$_4{}^-$, NO$_3{}^-$, ClO$_4{}^-$, CH$_3$CO$_2{}^-$, TCNQ$^-$),[27] but is smaller than that reported for the encapsulation compounds [AgIr$_2$(dmb)$_4$(DMSO)$_2$]$^{3+}$ (5.284 Å),[28] [AgIr$_2$(dmb)$_4$(PPh$_3$)$_2$]$^{3+}$ (5.284 Å),[29] and [Pd$_2$(μ-Cl)(dmb)$_4$]$^{3+}$ (5.428 Å).[20] The short d(AuAu) datum indicates the presence of bonding, and as stated above, this is one of the shortest ever reported for clusters. The other short Au−Au bonds are those of the binuclear [Au$_2$Pt$_2$-(PPh$_3$)$_4$(CN-xyxyl)$_4$](PF$_6$)$_2$ (2.593(2) Å),[2] Au^{II}(ylide)$_2$Cl$_2$ (2.597 Å),[30] Au$^0_2$(ylide)$_2$Br$_2$ (2.61 Å)[31] (ylide = (CH$_2$)$_2$P(C$_2$H$_5$)$_2{}^-$),

Table 3. IR-Active ν(CN) Data for Various Pt−CNR (Alkyl) Complexes[a]

compd	oxidation state	ν(CN) (cm^{-1})	ref
Pt$_3$(CN-t-Bu)$_6$	0	2150	*b*
[Pt$_4$(dmb)$_5$]Cl$_2$	0.5	2150	this work
[Pt$_4$(dmb)$_4$(PPh$_3$)$_2$]$^{2+}$	0.5	2146	this work
[Pt$_2$Au$_2$(dmb)$_2$(PPh$_3$)$_4$]$^{2+}$	I	2164	this work
Pt$_2$(dmb)$_2$Cl$_2$	I	2170^d	this work
Pt$_2$(dmb)$_2$Cl$_4$	II	2221	this work
[Pt$_2$(CN-t-Bu)$_3$(Cl)$_3$(μ-CN)]· Pt(CN-t-Bu)$_2$(Cl)$_2$	II	2217	*c*

[a] R = *tert*-butyl or dmb. [b] Green, M.; Howard, J. A.; Spencer, J. L.; Stone, F. G. A. *J. Chem. Soc., Chem. Commun.* **1975**, 3. [c] Harvey, P. D.; Truong, K. D.; Aye, K. T.; Drouin, M.; Bandrauk, A. D. *Inorg. Chem.* **1994**, *33*, 2347. [d] Average value between 2180 (s) and 2160 cm^{-1} (sh).

and Au$_2$((μ-C$_6$H$_4$)PPh$_2$)$_2$I$_2$ (av 2.593 Å)[32] and of the naked Au$_2$-(g) compounds:[33] Au$_2$($^1\Sigma_g{}^+$) = 2.472 Å, Au$_2$($^1\Sigma_u{}^+$) = 2.520 Å, and Au$_2$($^3\Sigma_u{}^+$) = 2.568 Å. In the latter cases, formal Au(II)−Au(II) and Au(0)−Au(0) single bonds are depicted. This distance also falls somewhat short in comparison to that of the related singly Au−Au bonded (Ph$_3$P)Au−Au(PPh$_3$) complex (2.76 Å).[34] In this case the PPh$_3$ ligands are not placed linear with the Au$_2$ bond, but adopt a trans geometry. For the Au(I)·· ··Au(I) species, separations commonly ranging from 2.90 to 3.54 Å have been reported (for examples, see: [Au$_2$(dmpm)$_2$]Cl$_2$ (dmpm = di(dimethylphosphino)methane), 3.010 Å,[35] [Au$_2$-(dmpm)$_2$](PF$_6$)$_2$, 3.044 Å,[36] Au$_2$(ylide)$_2$, 2.977 Å,[31] Au$_2$(tmb)-Cl$_2$ (tmb = 2,5-dimethyl-2,5-diisocyanohexane), 3.301 Å,[37] and Au$_2$(dmb)(CN)$_2$, 3.536 Å,[38] and others[39]). Due to the quasi-D_{2h} local symmetry of the cluster, and the simple ^{31}P NMR spectra, one cannot confidently claim the presence of a Au(I)−Au(III) bond in this case. Hence only two scenarios remain: both Au atoms are in either the II or 0 oxidation state. To determine this, one can monitor ν(CN) for various Pt−CNR (R = alkyl with environment very similar to dmb) as a function of the Pt oxidation state (Table 3). The IR-active ν(CN) bands for solid-state Pt(0) and Pt(0.5) species are located around 2148 ± 2 cm^{-1}, while they are at 2170 ± 10 cm^{-1} for Pt(I), and 2221 and 2217 cm^{-1} for Pt(II) complexes. The [Pt$_2$Au$_2$(dmb)$_2$-(PPh$_3$)$_4$]$^{2+}$ salt exhibits a strong IR absorption at 2170 cm^{-1} as well and clearly indicates the presence of Pt(I) metals, not Pt-(−I). In this case, the Au metals are in the formal oxidation state 0. Consequently, the bond order (BO) between the Pt and Au atoms would be 0.25. The Pt−Au BO is 0.33 for the trinuclear complex (NC)$_2$Pt$_2$(μ-AuCl)(μ-dppm)$_2$, and the d(PtAu) values are indeed shorter (2.633(2) and 2.648(2) Å).[24] It is interesting to note that the AuP distance is 2.317(2) Å and is significantly shorter than that found in Au$^0{}_2$(PPh$_3$)$_2$ (2.37 Å)[34]

(26) (a) Che, C.-M.; Herbstein, F. H.; Schaefer, W. P.; Marsh, R. E.; Gray, H. B. *Inorg. Chem.* **1984**, *23*, 2572. (b) Perreault, D.; Drouin, M.; Michel, A.; Harvey, P. D. *Inorg. Chem.* **1992**, *31*, 2740.

(27) (a) Fortin, D.; Drouin, M.; Harvey, P. D. *J. Am. Chem. Soc.* **1998**, *120*, 5351. (b) Perreault, D.; Drouin, M.; Michel, A.; Harvey, P. D. *Inorg. Chem.* **1992**, *31*, 3688.

(28) Sykes, A. G.; Mann, K. R. *J. Am. Chem. Soc.* **1988**, *110*, 8252.

(29) Sykes, A. G.; Mann, K. R. *Inorg. Chem.* **1990**, *29*, 4449.

(30) Schmidbaur, M.; Mandl, J. R.; Frank, A.; Muttner, G. *Chem. Ber.* **1976**, *109*, 466.

(31) Basil, J. D.; Murray, H. H.; Fackler, J. P., Jr.; Tocher, J.; Mazany, A. M.; Trycinska-Bancroft, B.; Knachel, H.; Dudis, D.; Delord, T. J.; Marder, D. O. *J. Am. Chem. Soc.* **1985**, *107*, 6908.

(32) Bennett, M. A.; Bargava, S. K.; Griffiths, K. D.; Robertson, G. B. *Angew. Chem., Int. Ed. Engl.* **1987**, *26*, 260.

(33) Huber, K. P.; Herzberg, G. *Molecular Spectra and Molecular Structure Constants of Diatomic Molecules*; Van Nostrand: New York, 1979.

(34) Mingos, D. M. P. *Pure Appl. Chem.* **1980**, *52*, 705.

(35) Kozelka, J.; Oswald, H. R.; Dubler, E. *Acta Crystallogr.* **1986**, *C42*, 1007.

(36) Perreault, D.; Drouin, M.; Michel, A.; Miskowski, V. M.; Schaefer, W. P.; Harvey, P. D. *Inorg. Chem.* **1992**, *31*, 695.

(37) Perreault, D.; Drouin, M.; Michel, A.; Harvey, P. D. *Inorg. Chem.* **1991**, *30*, 2.

(38) Che, C.-M.; Wong, W.-T.; Lai, T.-F.; Kwong, H.-L. *J. Chem. Soc., Chem. Commun.* **1989**, 243.

(39) Jaw, H.-R. C.; Savas, M. M.; Rogers, R. D.; Mason, W. R. *Inorg. Chem.* **1989**, *28*, 1028.
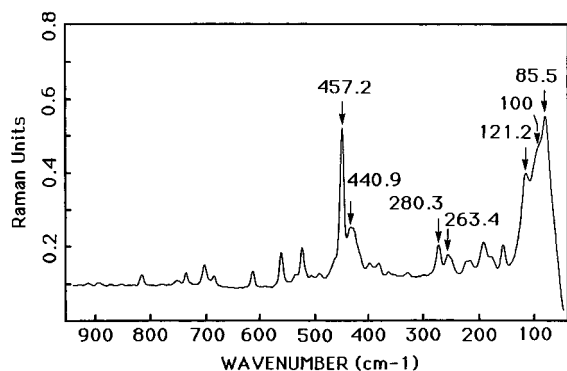
Figure 2. Solid-state FT-Raman spectrum of $[Pt_2Au_2(dmb)_2(PPh_3)_4]$-$(PF_6)_2$ at room temperature. Experimental conditions: 300 scans, 4 cm^{-1} spectral resolution.

and $Au^I(PPh_3)_3^+$ (2.40 Å, av).[40] Similarly, the PtP distance is 2.3612(19) Å and is significantly longer than that found for $Pt^0(PPh_3)_3$ (2.266 Å, av),[41] $Pt^0(PPh_3)_2(\eta^2\text{-}C_8H_{12})$ (2.266 Å, av.),[42] and $Pt^0(PPh_3)_2(\eta^2\text{-}C_6H_4)$ (2.268 Å, av).[43] These data are consistent with the fact that lower oxidation states lead to more M → P π back-bonding, and therefore shorter MP bonds, clearly indicating that the Pt metal is not in its reduced form (not Pt(0) or Pt(−I)). In addition the PtP distance of 2.3612(19) Å is surprisingly longer than that found in $Pt_2^I(\mu\text{-}C_6H_4PPh_2)_2(PPh_3)_2$ (2.30 Å), $Pt^{II}(PPh_3)_2(C≡CC(CH_3)_2(OH))$ (2.320 Å, av),[45] and $Pt^{II}(dppe)_2^{2+}$ (dppe = $Ph_2P(CH_2)_2PPh_2$; 2.334 Å, av). These very long PtP and very short AuP distances suggest that the electronic density at the Au atoms is indeed significantly greater than at the Pt atoms.

2. Raman Spectra. In order to address the amplitude of the Au_2 and PtAu interactions, the Raman spectra were acquired to extract $\nu(Au_2)$ and $\nu(PtAu)$ and estimate their respective force constants. The low-frequency spectrum for solid $[Pt_2Au_2(dmb)_2\text{-}(PPh_3)_4](PF_6)_2$ (Figure 2) exhibits three strong scatterings at 121.2, ~100, and 85.5 cm^{-1}, which are all reasonable candidates for $\nu(Au_2)$ and $\nu(AuPt)$ assignments. The larger frequency of the lower intensity peak at 121.2 cm^{-1} can only be associated with a stronger bond, which is apparent in the shorter Au−Au distance (2.60 Å). This assignment is consistent with literature data reported for the naked Au_2(g) and Au_2^-(g) species in their $^3\Sigma_u^+$ and $^2\Sigma_u^+$ electronic states, respectively, with Au_2 distances of 2.568[33] and 2.582 Å,[47] and $\nu(Au_2)$ of 142[33] and 149 cm^{-1},[47] respectively. Similarly, a high-frequency value for $\nu(Au_2)$ (162 cm^{-1})[48] has also been observed for the complex $Au_2(ylide)_2Cl_2$ where $d(Au_2)$ = 2.597 Å. The lower $\nu(Au_2)$ value for the mixed-metal cluster (121.2 cm^{-1}) is due to the presence of the heavy PPh$_3$ groups coordinated along the Au_2 bond.

For the following analysis, the knowledge of $\nu(MP)$ is necessary. Numerous literature data on M−PPh$_3$ complexes are known and place these frequencies <200 cm^{-1}.[49,50] For instance, $\nu(MP)$ for $(PPh_3)_2MX_2$ and $(PPh_3)MCl_3$ (M = Co, Ni, Zn; X = Cl, Br) ranges from 138 to 190 cm^{-1}.[51] Of particular interest, Jones and Powell[52] assigned $\nu(AuP)$ at 182 cm^{-1} for (PPh_3)-AuCl, and Che et al.[53] investigated the vibrational spectra of $(PPh_3)_2PtCl_2$ and located $\nu(PtP)$ at 200 and 171 cm^{-1}. In Figure 2, the peaks at 162.1 and 183.3 cm^{-1} correspond to $\nu(PtP)$ and $\nu(AuP)$, respectively. These assignments are based upon the longer (i.e., weaker) M−P bond for M = Pt (2.362(2) Å vs 2.317(2) Å for M = Au). The scatterings between 197 and 280 cm^{-1} are those of PPh$_3$.[49,52,54,55]

The $F(Au_2)$ value (metal−metal force constant) can now be estimated using the following equations applied to the linear P−Au−Au−P fragment:[56]

$$\lambda_1 + \lambda_2 = \frac{2F(Au_2)}{M(Au)} + \left[1 + \frac{M(P)}{M(Au)}\right]\left[\frac{F(Au_2)}{M(Au)}\right] \quad (2)$$

$$\lambda_1\lambda_2 = 2\left[\frac{2F(Au_2)F(AuP)}{M(Au)M(P)}\right] \quad (3)$$

where $\lambda_i = (2\pi c\nu_i)^2$ (c = speed of light) with ν_1 and ν_2 being the Raman-active $\nu(Au_2)$ and $\nu(AuP)$ totally symmetric modes, and M = mass. The resolution of eqs 2 and 3 gives an equation of a quadratic form, which provides two solutions. For comparison purposes all three low-frequency data (121.2, 100, and 85.5 cm^{-1}) were used for ν_1, and the results are as follows: for ν_1 = 121.2 cm^{-1}, $F(Au_2)$ = 1.21 and 1.60 mdyn Å^{-1}; for ν_1 = 100 cm^{-1}, $F(Au_2)$ = 1.80 and 0.73 mdyn Å^{-1}; and for ν_1 = 85.5 cm^{-1}, $F(Au_2)$ = 1.86 and 0.52 mdyn Å^{-1}. The last two entries do not provide reasonable values for F, as they are either too small or two large, in comparison with literature data for Au_2-bonded species of similar bond distances (i.e., $Au_2^-(^2\Sigma_u^+)$, F = 1.29 mdyn Å^{-1}; $Au_2(^3\Sigma_u^+)$, F = 1.18 mdyn Å^{-1}).[33] Recently empirical relationships between metal−metal distances (in Å) and $F(M_2)$ (in mdyn Å^{-1}) applied to homonuclear bi- and polynuclear complexes have been reported.[57] For Au_2 species this equation is as follows:

$$d(Au_2) = -0.290 \ln F(Au_2) + 2.68 \qquad (\sigma = 0.96) \quad (4)$$

with σ being the correlation coefficient. Such relations generally give an agreement between the calculated and experimental values that falls within ±0.05 Å. By calculating $d(Au_2)$ for each F value extracted above, eq 4 provides the following results: for ν_1 = 121.2 cm^{-1}, $d(Au_2)$ = 2.62 and 2.54 Å; for ν_1 = 100 cm^{-1}, $d(Au_2)$ = 2.51 and 2.77 Å; for ν_1 = 85.5, $d(Au_2)$ = 2.50 and 2.87 Å, in the same order listed above. On the basis of the comparison between the calculated and experimental $d(Au_2)$

(40) Jones, P. G. *J. Chem. Soc., Chem. Commun.* **1980**, 1031.
(41) Chaloner, P. A.; Hitchcock, P. B.; Broadwood-Strong, G. T. L. *Acta Crystallogr., Sect. C* **1989**, *45*, 1309.
(42) Robertson, G. B.; Whimp, P. O. *Aust. J. Chem.* **1980**, *33*, 1373.
(43) Robertson, G. B.; Whimp, P. O. *J. Am. Chem. Soc.* **1975**, *97*, 1051.
(44) Bennett, M. A.; Berry, D. E.; Bhargava, S. K.; Ditzel, E. J.; Robertson, G. B.; Willis, A. C. *J. Chem. Soc., Chem. Commun.* **1987**, 1613.
(45) Furlani, A.; Licoccia, S.; Russo, M. V.; Villa, A. C.; Guastini, C. *J. Chem. Soc., Dalton Trans.* **1984**, 2197.
(46) Engelhardt, L. M.; Patrick, J. M.; Raston, C. L.; Twiss, P.; White, A. H. *Aust. J. Chem.* **1984**, *37*, 2193.
(47) Bauschlicher, C. S., Jr.; Langhoff, S. R.; Partridge, H. *J. Chem. Phys.* **1989**, *91*, 2412 and the references therein.
(48) Farell, F.; Spiro, T. G. *Inorg. Chem.* **1971**, *10*, 1606.
(49) Nakamoto, K. *Infrared and Raman Spectra of Inorganic and Coordination Compounds*, 4th ed.; New York, 1986; p 338 and the references therein.
(50) Clark and Hempleman investigated the resonance Raman spectra of $Rh_2(O_2CR)_4(PPh_3)_2$ complexes and concluded that $\nu(RhP)$ is <200 cm^{-1}, in the following: Clark, R. J. H.; Hempleman, A. J. *Inorg. Chem.* **1989**, *28*, 746.
(51) Bradbury, J.; Forest, K. P.; Nuttall, R. H.; Sharp, D. W. A. *Spectrochim. Acta* **1967**, *23A*, 2701.
(52) Jones, A. G.; Powell, D. B. *Spectrochim. Acta* **1974**, *30A*, 563.
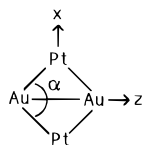(53) Che, X.; Song, G.; Li, T. *Acta Chim. Sin.* **1989**, *47*, 969.
(54) Shobatake, K.; Postmus, C.; Farraro, J. R.; Nakamoto, K. *Appl. Spectrosc.* **1969**, *23*, 12.
(55) Garcia Figueroa, E.; Cabrera, A.; Alvarez, C.; Gomez Lara J. *Rev. Inst. Mex. Pet.* **1974**, *6*, 25.
(56) Herzberg, G. *Infrared and Raman Spectra of Polyatomic Molecules*; Van Nostrand Reinhold Co.: New York, 1945; p 181.
(57) Harvey, P. D. *Coord. Chem. Rev.* **1996**, *153*, 175 and the references therein.

Chart 4

values, the assignment $\nu(Au_2) = 121.2$ cm^{-1} is appropriate. The 1.21 mdyn Å^{-1} F value is preferred as it compares more favorably to literature data for similar bond distances (see above), and the calculated d value (2.62 Å) falls well within the 0.05 Å limit generally encountered for eq 4.

For a cyclic M_2M_2' flattened butterfly (D_{2h}; Chart 2), there are six vibrational modes: $2a_g + b_{2g} + b_{1u} + b_{2u} + b_{3u}$. The two Raman-active $\nu(PtAu)$ modes are a_g and b_{2g} (100 and 85.5 cm^{-1}), while $\nu(Au_2)$ is of a_g symmetry. The equation relating $\nu(MM')$ and $F(MM')$ for a M_2M_2' D_{2h} frame (Chart 4) is given by[58]

$$\lambda(b_{2_g}) =$$
$$\frac{2F(MM')\{\sin(\alpha/2) + [(M_M/M_{M'})(\cos^2(\alpha/2))]/\sin(\alpha/2)\}}{M_M(1 + M_M/M_{M'})\cot^2(\alpha/2)} \quad (5)$$

where M_M and $M_{M'}$ = mass for Au and Pt, respectively, and $\alpha = \angle PtAuPt$ (125.261°). Equation 5 computes $F(PtAu) = 0.67$ and 0.49 mdyn Å^{-1} for $\nu = 100$ and 85.5 cm^{-1}, respectively. There is no empirical relationship that correlates $d(PtAu)$ with $F(PtAu)$. It was recently proposed to use the average values of both the slopes and intercepts in these equations for homonuclear systems. In these cases, the difference between the calculated and experimental values was greater (± 0.09 Å) for the worse comparisons. For M = Pt, the homonuclear equation is[57]

$$d(Pt_2) = -0.233 \ln F(Pt_2) + 2.86 \qquad (\sigma = 0.98) \quad (6)$$

For heteronuclear PtAu systems, such an equation reads

$$d(PtAu) = -0.257 \ln F(PtAu) + 2.77 \quad (7)$$

With $F(PtAu) = 0.67$ and 0.49 mdyn Å^{-1}, eq 7 computes $d(PtAu) = 2.87$ and 2.95 Å, respectively. The comparison with the experimental value (2.82 Å) is reasonable for the datum $\nu = 100$ cm^{-1}, but is clearly inappropriate for $\nu = 85.5$ cm^{-1}. We assign the b_{2g} and a_g $\nu(PtAu)$ modes to 100 and 85.5 cm^{-1}, respectively. Incidentally, a recent report on a naked K_4 cluster that also exhibited a flattened butterfly geometry established that the Raman-active $\nu(KK)$ modes vary as $a_g(K-K$ edge sharing band) > b_{2g} > a_g,[59] consistent with our findings.

The $\nu(PtC)$ peaks are found at 457.2 and 440.9 cm^{-1}. The remainder of the spectra are associated with intraligand and PF$_6^-$ vibrations and are not interpreted further.

3. MO Analysis. EHMO computations were performed in order to qualitatively predict the electronic structure of the Pt₂-Au₂(CNCH₃)₄(PH₃)₄²⁺ fragment. The analysis is performed using the interactions between two Pt(CNCH₃)₂(PH₃)⁺ fragments with the H₃PAu⁰−Au⁰PH₃ center. Gilmour and Mingos described the nature of the frontier orbitals in T-shaped PtL₃⁺ species and the Au₂L₂ fragment,[3] where L is the 2e⁻ H⁻ donor. The former fragment is isolobal with AuPR₃, H, and CH₃ as well as any other fragments which possess only a singly

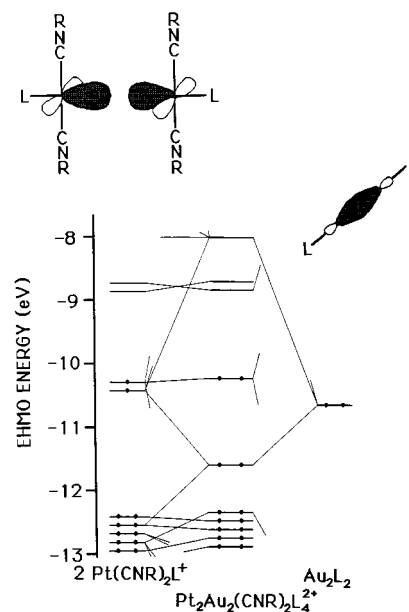(58) Perreault, D.; Drouin, M.; Michel, A.; Harvey, P. D. *Inorg. Chem.* **1993**, *32*, 1903.
(59) Kornath, A.; Lugwig, R.; Zoermer, A. *Angew. Chem., Int. Ed.* **1998**, *37*, 1575.

Figure 3. Walsh diagram showing the interactions between two Pt-(CNCH₃)₂(PH₃)⁺ fragments with Au₂(PH₃)₂. Contributions of 1% or less are not presented.

occupied frontier orbital of a_1 symmetry. This a_1 orbital is mainly composed of a dp hybrid pointing toward the missing vertex of the Pt square-planar coordination polygon. The latter fragment (Au₂L₂) exhibits a σ_g Au−Au bonding using in-phase sp$_z$ coordination on each gold leading to stronger Au₂ σ-bonding. At higher energy, the π-sets form the in-phase (LUMO) and out-of-phase (π_g*) combinations of the six p$_x$ and six p$_y$ orbitals.[3] Overall the bonding scheme is best described by two sets of three-center two-electron bonds. The interaction diagram between two PtL₃⁺ and Au₂L₂ fragments readily predicts that the LUMO and HOMO will be solely composed of M orbitals. However, the L = H⁻ model does not include the presence of accessible π* orbitals from the C≡N−R groups. In fact, recent DFT (density functional theory) calculations on M(CNH)₄⁺ species (M = Ag, Cu) demonstrated that the LUMO was located within the CNR centers.[60] Further EHMO calculations on closely related Ag₂(dmb)₂X₂ complexes (X = Cl, Br, I) also lead to the same conclusions.[61]

The overall results for the model complex Pt₂Au₂(CNCH₃)₄-(PH₃)₄²⁺ are presented in Figure 3 and Table 4. Most of the computational results are consistent with the findings of Gilmour and Mingos,[3] except that the LUMO is clearly predicted to be an MO mainly composed of CNR π* orbitals. A brief description of the frontier MO is now provided. The LUMO and LUMO + 1 are quasi-degenerated MO's (ΔE < 0.1 eV) localized mainly within the π*(C≡N) fragments (using the p$_z$ atomic orbitals), and they exhibit some minor Pt p$_z$ atomic contributions as well. These sets of MO's are perpendicularly oriented to the Pt₂Au₂ plane. About 1 eV above the LUMO lies an empty MO (LUMO + 2) that exhibits a strong mixture between the in-plane Pt₂Au₂ fragment and a π*(CNR) set. The latter originates from the interactions between the two in-phase a_1 orbitals of the Pt(CNCH₃)₂(PH₃)⁺ fragments, and the HOMO of the Au₂L₂ moiety. The negative overlaps between the two lead to an antibonding Pt−Au interaction in this MO. The HOMO originates from out-of-phase interactions between 2 Pt-(CNCH₃)₂(PH₃)⁺ as major components, with the Au p$_z$ atomic

Table 4. Atomic Contributions for Selected MO's of the $Pt_2Au_2(CNCH_3)_4(PH_3)_4{}^{2+}$ Model Complex[a]

MO no.	EHMO energy (eV)	%Pt					%Au			%P		%C		%N		comments/assignments	D_{2h} local sym
		s	p_x	p_z	d_{z^2}	$d_{z^2y^2}$	s	p_x	p_z	p_x	p_z	p_x	p_z	p_x	p_z		
54	−7.753				6	4	14		10			14		20		$\sigma(Au_2) + \sigma^*(PtAu)/\pi^*(CNR)$, mixed	a_g
55	−8.628			20									46		28	$\pi^*(CNR)$ mainly	b_{1u}
56	−8.701			22									44		28	$\pi^*(CNR)$ mainly, LUMO	b_{2g}
57	−10.207	10	16		22	10	10			8		4		4		$\sigma(PtAu)$ mainly, HOMO	b_{3u}
58	−11.601	6	10		4	12	22				10					$\sigma(Au_2) + \sigma(PtAu)$	a_g

[a] Contributions <1% not included.
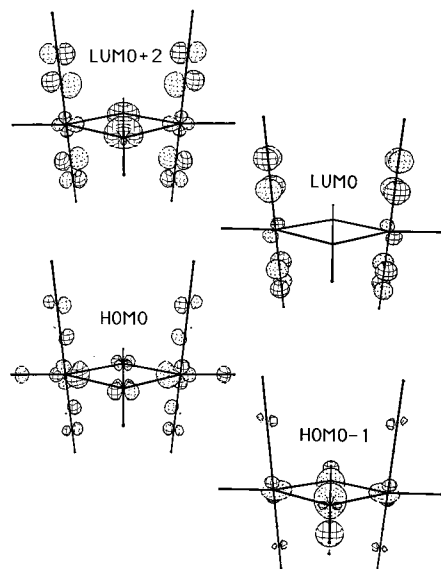
Figure 4. CACAO representations for the HOMO − 1, HOMO, LUMO, and LUMO + 2 of the $Pt_2Au_2(CNCH_3)_2(PH_3)_4{}^{2+}$ model cluster.

orbitals, leading to a somewhat Pt−Au bonding orbital. Contributions from the :P lone pairs located along the Pt⋯Pt axis and π*(C≡N) orbitals are also computed in this case. Below lies the HOMO − 1, which is also built upon interactions between the two in-phase orbitals of the $Pt(CNCH_3)_2(PH_3)^+$ fragments, and the HOMO of the Au_2L_2 moiety. In this case positive overlaps between the two generate Pt−Au bonding interactions. In addition, contributions from the Pt s and p_x orbitals are computed in order to promote further Pt−Au bonding interactions. In reverse, there are few if any contributions from the π*(C≡N) sets. This result is easily explained by the larger gap between this MO and the π*(C≡N) orbitals. Below these MO's lie a series of MO's which are localized within the d-block of the Pt (higher energy) and Au (lower energy) metals. These are not discussed in this work.

4. UV−Vis Spectra. The UV−vis spectra of the green $Pt_2Au_2(dmb)_2(PPh_3)_4{}^{2+}$ cluster in solution are characterized by three series of absorptions in the visible region (Figure 5): a weak absorption between 600 and 700 nm, a well "isolated" narrow band at around 520 nm, and another band at around 400 nm located on the red side of a series of stronger absorptions between 280 and 400 nm. Absorption bands arising from dσ → dσ* transitions in M_2 σ-banded compounds, or from dσ* → pσ transitions in M_2 face-to-face and non-M_2-bonded dimers, generally undergo a significant decrease in fwhm with the decrease in temperature. Examples for such phenomena are numerous in the literature, notably for d^7−d^7 and d^9−d^9
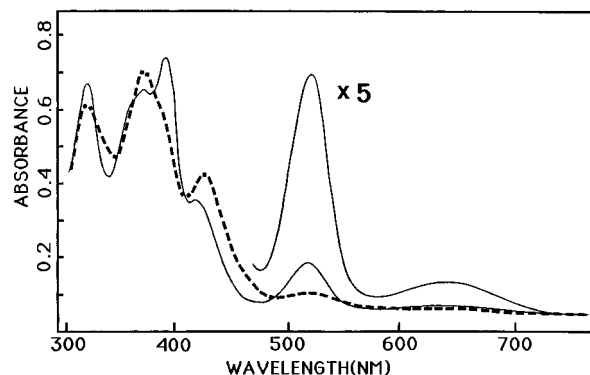
Figure 5. Absorption spectra of $Pt_2Au_2(dmb)_2(PPh_3)_4{}^{2+}$ (as a PF_6- salt) in butyronitrile at 298K (− − −) and 77 K (—).

σ-bonded M_2 species,[62,63] and for non-M_2-bonded dimers, such as the d^8−d^8 and d^{10}−d^{10} compounds.[61,64,65] This change in fwhm is associated with the presence of low-frequency Franck−Condon active vibrational modes, which upon warming allow the population of vibrationally excited levels in the ground state to give rise to "hot bands" in the spectra according to a Boltzmann distribution. Upon cooling, these levels are less populated and fwhm decreases. Such modes are generally $\nu(M_2)$, and on some occasions $\nu(ML)$ if L is heavy or weakly bonded (then $\nu(ML)$ is small) and, of course, is active in the Franck−Condon term. A good description of this phenomenon can be found in ref 66. Higher energy modes could be Franck−Condon active, such as intraligand modes, but there would not be significant change in fwhm. Upon cooling of the samples from room temperature to 77 K, some absorption bands significantly sharpen, but others do not. This is the case for the peak located at 514 nm and those below 400 nm, but much less for the 640 nm band. The data are presented in Table 5 (solvent = butyronitrile) and are as follows for the two lowest energy absorption bands (band 1, ~640 nm; band 2, ~515 nm): band 1 fwhm = 2360 and 2100 cm^{-1}, band 2 fwhm = 2400 and 1400 cm^{-1}, for T = 298 and 77 K, respectively. The data clearly indicate that band 2 must arise from a M_n-localized electronic transition. The relatively small decrease in fwhm for band 1 indicates that the frequencies of some of the Franck−Condon active modes must be large. The presence of $\nu(PtC)$ (~450 cm^{-1}) would be consistent with this behavior and would indicate the presence of an MLCT. Indeed literature data shows that the fwhm for MLCT bands for the $M_2(dba)_3$ complexes (M = Pd, Pt; dba = dibenzylideneacetone) does not change very much from 295 to 77 K, although the λ_{max} may change slightly.[67] On

(60) Fortin, D.; Drouin, M.; Turcotte, M.; Harvey, P. D. *J. Am. Chem. Soc.* **1997**, *119*, 531.

(61) Piché, D.; Harvey, P. D. *Can. J. Chem.* **1994**, *72*, 705.

(62) For examples, see: (a) Harvey, P. D.; Johnston, P.; Coville, N. J. *Can. J. Chem.* **1994**, *72*, 2176 and the references therein. (b) Harvey, P. D.; Butler, I. S.; Barreto, M. C.; Coville, N. J.; Harris, G. H. *Inorg. Chem.* **1988**, *27*, 639 and the references therein.

(63) Harvey, P. D.; Murtaza, Z. *Inorg. Chem.* **1993**, *32*, 4721.

(64) Smith, D. M. Ph.D. Dissertation. California Institute of Technology, 1989.

(65) Harvey, P. D.; Gray, H. B. *J. Am. Chem. Soc.* **1988**, *110*, 2145.

Table 5. UV−Vis Spectroscopic Data[a]

band no.	298 K				77 K		
	λ_{max} (± 2 nm)	ν_{max} (cm^{-1})	fwhm (± 100 cm^{-1})	ϵ (M^{-1} cm$^{-1} \pm 5\%$)	λ_{max} (± 2 nm)	ν_{max} (cm^{-1})	fwhm (± 100 cm^{-1})
1	655	$15\,270 \pm 50$	2360	8.34×10^2	639	$15\,650 \pm 50$	2100
2	516	$19\,380 \pm 50$	2400	2.86×10^3	514	$19\,460 \pm 80$	1400
3	418	$23\,920 \pm 110$		2.15×10^4	410	$24\,390 \pm 110$	
4	366	$27\,320 \pm 150$		3.78×10^5	382	$26\,180 \pm 140$	
					362	$27\,620 \pm 150$	
5	316	$31\,650 \pm 200$		3.23×10^5	314	$31\,850 \pm 200$	

[a] Butyronitrile.
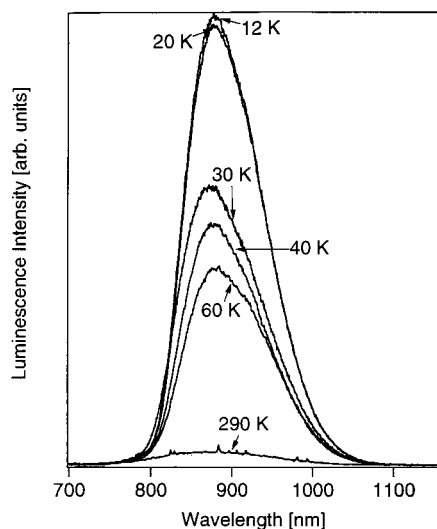
Figure 6. Solid-state emission spectra of solid [Pt₂Au₂(dmb)₂(PPh₃)₄]-(PF₆)₂ as a function of temperature ($\lambda_{exc} = 630$ nm).

the basis of the ϵ data (Table 5), band 1 ($\epsilon = 834$ M^{-1} cm^{-1}; 298 K) is a partially allowed transition.[68] Due to the presence of the heavy Pt and Au metals, strong spin−orbit coupling occurs,[68] and electronic bands with ϵ ranging in the several hundred M^{-1} cm^{-1} are also likely to appear in the spectra. The scope of this work does not allow us to address this.

For the remainder of the spectra, the ϵ data and the significant decrease in fwhm with the lowering of the temperature indicate that the intense bands must arise from M$_n$-centered transitions. Reasonable candidates for such transitions are HOMO − n → LUMO + 2 (Figure 3), where HOMO − n are MO's localized mainly within the Pt metals. For secure assignments, measurements of polarized absorption spectra of single crystals are clearly necessary.

5. Emission Spectra. While the cluster is not luminescent in solutions at room temperature, luminescence is detected in the red region of the spectra in the solid state between 298 and 12 K ($\lambda_{max} \sim 875$ nm; Figure 6) and in frozen solutions (77 K). The excitation spectra are superimposable on the absorption spectra, and the 77 K emission lifetime in this case is 4.4 $\pm$ 0.4 ns (solvent = butyronitrile).[69] This value is short, but not unprecedented. For instance the related 58-electron tetranuclear

cluster Pt₄(dmb)₄(PPh₃)₂²⁺ and corresponding diphosphine polymers ({Pt₄(dmb)₄(PPh₂(CH₂)$_m$PPh₂)²⁺}$_n$ (m = 4, 5, 6)) exhibit emission λ_{max} of 730−750 nm and τ_e of 2.71−5 ns.[20] The Stokes shift ($\sim$4200 cm^{-1}) is significantly larger than that observed for the fluorescence emissions in Pt₂(POP)₄⁴⁻ (POP = P₂O₅H₂²⁻; $\sim$2800 cm^{-1}),[70] [Ir₂(M′)(CO)₂X₂(μ-dpma)₂]Y (M′ = PbI, PbNO₃, SnCl, TlNO₃, SbF₂; X = Cl, Br, I; Y = PF₆⁻, NO₃⁻, nil; dpma = {(Ph₂PCH₂)₂AsPh}₂; $\sim$800 < Stokes shift < 2100 cm^{-1}),[71] [Au₂Ir(CO)(μ-dpma)₂](PF₆)₂ ($\sim$1760 cm^{-1}),[72] and [Ir₂(SnCl)(CO)₂Cl₂(μ-dpma)₂](SnCl₃) ($\sim$1500 cm^{-1}).[73] Knowing that τ_e (4.4 ns) is $\sim$3 orders of magnitude larger than that of Pt₂(POP)₄⁴⁻ fluorescence for instance ($\sim$8 ps, at 298K in H₂O),[70] and that the Stokes shift is somewhat large, the emission for Pt₂Au₂(dmb)₂(PPh₃)₂²⁺ is assigned to a phosphorescence. To our knowledge this emission is the lowest energy ever reported for Pt and Au species.[67,74,75] An explanation for this can be found in the nature of the HOMO. By the fact that the out-of-phase combination of the a₁ orbital of the Pt-(CNR)₂(PR′₃)⁺ fragments does not interact strongly with the Au₂L₂ moiety (see details in Table 4), very little perturbation of the MO energy is felt with respect to that of the out-of-phase combination MO itself (Figure 3). Similarly the π*(CNR) MO's do not interact with the Au₂L₂ fragment. As a consequence, the HOMO−LUMO energy gap will be small. Qualitatively, the HOMO is largely localized within the Pt metals, and the LUMO within the π*(CNR) system. Since both the HOMO−LUMO energies differ and their atomic contributions are similar (i.e., comparison between the HOMO and LUMO for both 2 Pt(CNR)₂(PR′₃)⁺ moieties and the Pt₂Au₂(CNR)₄(PR′₃)₄²⁺ cluster), the absorption spectra for both the "Pt(CNCH₃)₂-(PPh₃)⁺" fragment and [Pt₂Au₂(dmb)₂(PPh₃)₄]²⁺ are predicted to be very similar.

(66) Mickowski, V. M.; Smith, T. P.; Loehr, T. M.; Gray, H. B. *J. Am. Chem. Soc.* **1985**, *107*, 7925 and the references therein.
(67) Harvey, P. D.; Adar, F.; Gray, H. B. *J. Am. Chem. Soc.* **1989**, *111*, 1312.
(68) Turro, N. J. *Modern Molecular Photochemistry*; Benjamin/Cumming Pub. Co.: Menlo Park, 1978.
(69) The emission spectrum on the Fluorolog instrument exhibits a λ_{max} $\sim$834 nm, in comparison with Figure 6, which exhibits a band with λ_{max} at $\sim$875 nm, using a different detector (PMT Hamamatsu R406). The λ_{max} $\sim$834 nm band is located near the long-wavelength limit of the PMT and may not be appropriately corrected by the instrument software. The lifetime was measured at $\sim$830 nm on the PTI instrument. The corrected spectra in Figure 6 are more reliable spectra.
(70) Stiegman, A. E.; Rice, S. F.; Gray, H. B.; Miskowski, V. M. *Inorg. Chem.* **1987**, *26*, 1112.
(71) Balch, A. L.; Catalano, V. J.; Chatfield, M. A.; Nagle, J. K.; Olmstead, M. M.; Reedy, P. E., Jr. *J. Am. Chem. Soc.* **1991**, *113*, 1252.
(72) Balch, A. L.; Catalano, V. J.; Olmstead, M. M. *J. Am. Chem. Soc.* **1990**, *112*, 2010.
(73) Balch, A. L.; Olmstead, M. M.; Oram, D. E.; Reedy, P. E., Jr.; Reimer, S. H. *J. Am. Chem. Soc.* **1989**, *111*, 4021.
(74) Examples for emission data of Au$_n$ species can be found in the following: (a) Vickery, J. C.; Olmstead, M. M.; Fung, E. Y.; Balch, A. L. *Angew. Chem., Int. Ed. Engl.* **1997**, *36*, 1179. (b) Tzeng, B.-C.; Chan, C.-K.; Cheung, K.-K.; Che, C.-M.; Peng, S. M. *Chem. Commun.* **1997**, 135. (c) Hanna, S. D.; Khan, S. I.; Zink, J. I. *Inorg. Chem.* **1996**, *35*, 5813.

A further decrease of the solid sample temperature down to 12 K did not yield to improvement in spectral resolution (or change in fwhm) (Figure 6). The emission band is weakly asymmetric, where a shoulder is seen at ~920 nm (Δ between 875 and 920 nm is ~560 cm^{-1}). The relative intensity of the maximum and shoulder remains constant with temperature, which indicates that this shoulder could be of vibronic origin. If this is the case, then a PtAu $\rightarrow$ π*(CNR) charge transfer (MM'LCT) assignment would be appropriate for the emission. Higher resolution spectra are necessary to obtain a secure assignment.

---

(75) Examples for emission data of Pt$_n$ species can be found in the following: (a) Harvey, P. D. *J. Cluster Sci.* **1993**, *4*, 377 and the references therein. (b) Harvey, P. D.; Hubig, S. M.; Ziegler, T. *Inorg. Chem.* **1994**, *33*, 3700. (c) Zhang, T.; Drouin, M.; Harvey, P. D. *J. Cluster Sci.* **1998**, *171*, 351.

Supporting Information Available: Tables listing detailed crystallographic data, atomic positions, parameters, and bond lengths and angles and tables listing mass FAB fragments for the four compounds. This material is available free of charge via the Internet at http://pubs.acs.org.

IC981187M